Study on Dynamic Error Compensation of Laser Emitter for Digging Navigation System

Jingdao Fan

***Abstract*—Laser emitters are used to generate vertically intersecting structured light, which can provide a reference for pose measurement. Therefore, the accuracy of the pose measurement system is determined by the accuracy of laser emitter instruments. The motion joint errors of the mechanical structure of the laser emitter instrument are analyzed and the transverse and longitudinal error transmission models are established in this paper. On this basis, the dual-axis coupling model is established and the error simulation analysis is performed. A method of using spring traction for error compensation is proposed and compared with the error before compensation. The results show that the error is significantly reduced, and the average laser deflection angle is about 1/14 of the pre compensation value.**

***Index Terms*—Cross laser, error transmission, dual-axis coupling, error compensation.**

I. Introduction

THE laser emitter system is used to measure the position and orientation of excavation equipment in coal mine tun-nels. It consists of a laser emitter instrument, laser receivers and industrial controller [1], as shown in Fig. 1. The laser emitter instrument is fixed on the tunnel roof and emits orthogonal structured light forward as a reference.

The laser receiver is fixed on the measured equipment. The structured light projects onto the laser receiver, generating several light spots. When the pose of equipment changes, the readings of the light spots on the laser receiver also change accordingly. By analyzing the position readings of the light spots, the laser receiver's pose, which represents the measured equipment's pose, is calculated [2].

Currently, there are two methods to convert a laser beam into a planar laser: Powell prism [3] and rotating laser method [4]. The Powell prism has a divergence angle, and as the measurement distance increases, the radiation intensity of the light source decreases sharply. With a divergence angle of 5°, the radiation intensity of the planar laser at a distance of 100 meters is only 0.3% of that of a point laser beam [5]. Although increasing the power of the laser diode can improve its effective range, excessive power does not meet the safety standards of coal mines and can reduce the laser emitter's battery life.

Manuscript received 9 December 2023; revised 21 February 2024; accepted 17 March 2024. Date of publication 20 March 2024; date of current version 1 April 2024.

The author is with the Shaanxi Yanchang Petroleum (Group) Company Ltd., Xi'an 710065, China, and also with the Innovation Center of Intelligent Mining Technology in Coal Mine, State Administration of Work Safety, Huangling 727307, China (e-mail: 2876481044@qq.com).

Digital Object Identifier 10.1109/JPHOT.2024.3379559

This paper proposes using a rotating mechanism instead of an optical prism to generate a planar laser, as shown in Fig. 2. The mechanism consists of a rotating motor, a reflective mirror, and a laser diode. The laser diode and the rotating motor are fixed inside a base and aligned along the axis. The 45° reflective mirror is fixed on the rotating motor and rotates at a constant speed. The reflected light source forms a rotating 360° laser plane. This method increases the radiation intensity of the light spot at long distances, thereby improving the effective detection range of the navigation system. The accuracy of the emitted structured light determines the measurement accuracy of the system. Moreover, as the measurement distance increases, even small angular deviations can lead to significant position measurement errors. Therefore, improving the accuracy of the laser emitter instrument becomes crucial.

According to the standard, the positioning accuracy of ordinary laser emitters used for positioning is 1.5–4 mm, but such laser emitters do not have automatic adjustment function [6]. Xiang proposed a self-balancing laser horizontal positioning design with a comprehensive positioning accuracy of 3.3 mm [7]. Liu proposed a laser level module based on PID automatic adjustment, with a horizontal and vertical positioning accuracy of 1 mm [8]. However, the effective distance of this module is less than 5 m, which cannot meet the navigation requirements for mining purposes. Abdulla proposed a laser positioning method based on closed-loop control, with a positioning accuracy of ± 7 mm at 340 m [9].

The method proposed in this article will be analyzed in the following chapters. The error transmission model is built in chapter II, the dual-axis coupling model is promoted in chapter III, the error compensation analysis is made in chapter IV, and the chapter V draws the conclusions.

II. Error Transmission Model

The distribution of motion joint error clearances in the laser emitter device is shown in Fig. 3. The bearing clearance of the rotating motor is very small, and the standby reverse clearance of the stepper motor only has errors during motor startup and reverse rotation. Therefore, the error transmission model only considers the influence of two rotational joint clearances and two sliding joint clearances.

The rotational joint clearances cause the axis pin to undergo additional rotations around the three rotational degrees of freedom in addition to its intended rotational motion. This additional rotation is called rotational error, which refers to

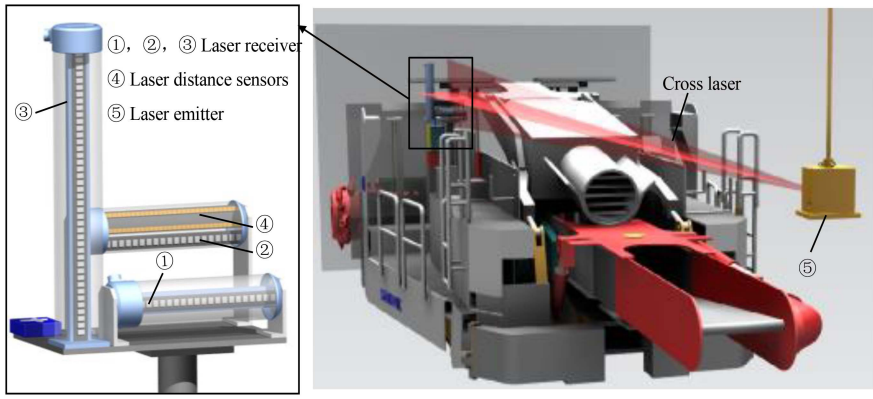

Fig. 1. Navigation system components.

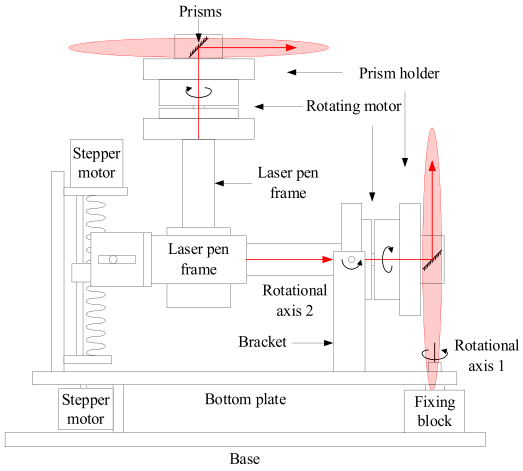

Fig. 2. Laser emitter principle.

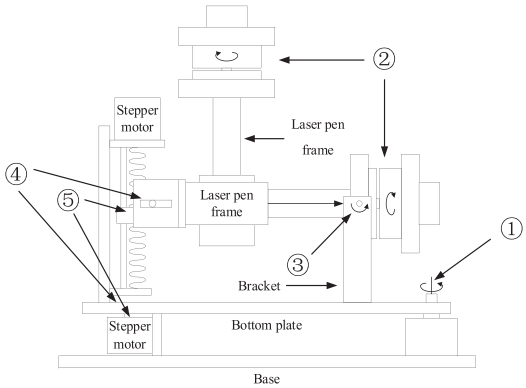

Fig. 3. Laser emitter clearances distribution. ① Rotational sub-clearance between the bottom plate rotational axis and the bottom plate;② clearance of the rotating bearings of the two rotating motors;③ rotational sub-clearance between the bracket and the rotating shaft that holds the laser pen frame in place;④ slip joint clearance between the two slots and the axis pin;⑤ stepper motor standby backlash

the extra rotational motion of the shaft pin relative to the axle hole in the three rotational directions $\Delta\varphi x^i$, $\Delta\varphi y^i$, $\Delta\varphi z^i$. The simplified model of rotational joint clearances is shown in Fig. 4. Firstly, a fixed coordinate system O_i-$x_iy_iz_i$ is established along

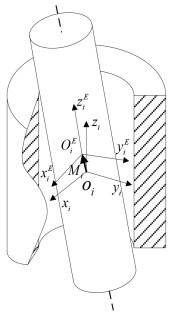

Fig. 4. Clearance model of rotating joint.

the axis line of the hole, and then a moving coordinate system $O_i^E - x_i^E y_i^E z_i^E$ is established along the axis line of the shaft, with the directions of the hole and shaft axis as the Z-axis direction. Without rotational joint clearance, the fixed coordinate system O_i-$x_iy_iz_i$ coincides with the moving coordinate system $O_i^E - x_i^E y_i^E z_i^E$; with rotational joint clearance, there may be three axial displacements and rotations between the coordinate systems $O_i^E - x_i^E y_i^E z_i^E$ and O_i-$x_iy_iz_i$ [10].

The vector M_i, pointing from the origin O_i to the origin O_i^E, represents the three small movements of the shaft pin coordinate system $O_i^E - x_i^E y_i^E z_i^E$ along the x_i, y_i and z_i directions of the fixed coordinate system O_i-$x_iy_iz_i$. Assuming the displacements along the x_i, y_i and z_i directions are Δx_i, Δy_i and Δz_i, respectively, the translational error component of the rotational joint clearance error can be represented by the transformation matrix M_i (Δx_i, Δy_i, Δz_i).

$$Mi(\Delta x_i, \Delta y_i, \Delta z_i) = \begin{bmatrix} 1 & 0 & 0 & \Delta x_i \\ 0 & 1 & 0 & \Delta y_i \\ 0 & 0 & 1 & \Delta z_i \\ 0 & 0 & 0 & 1 \end{bmatrix} \tag{1}$$

The rotational errors of the shaft pin coordinate system $O_i^E - x_i^E y_i^E z_i^E$, which are generated by rotations around the x_i, y_i, and z_i axes of the fixed coordinate system O_i-$x_iy_iz_i$, can be described using the *RPY* angle method. Assuming the angles of rotation of the shaft pin coordinate system $O_i^E - x_i^E y_i^E z_i^E$ around the x_i, y_i, and z_i axes are $\Delta\varphi_x^i$, $\Delta\varphi_y^i$, and $\Delta\varphi_z^i$,

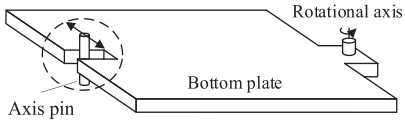

Fig. 5. Bottom plate movement model.

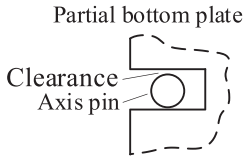

Fig. 6. Bottom plate friction joint.

respectively, the rotational error component of the rotational joint clearance error can be represented by the transformation matrix $RPY(\Delta\varphi_x^i, \Delta\varphi_y^i, \Delta\varphi_z^i)$. (2) shown at the bottom of this page.

In the above formulas, *c* represents the cosine function, and *s* represents the sine function.

By multiplying the translational error transformation matrix $M(\Delta x_i, \Delta y_i, \Delta z_i)$ and the rotational error transformation matrix $RPY(\Delta\varphi_x^i, \Delta\varphi_y^i, \Delta\varphi_z^i)$ of the rotational joint clearance, the error transformation matrix Ei of the rotational joint clearance can be obtained. (3) shown at the bottom of this page.

The given statement suggests that the actual values of the rotational angles $\Delta\varphi_x^i, \Delta\varphi_y^i$, and $\Delta\varphi_z^i$ in the rotational joint errors are very small. Therefore, by substituting $\sin\Delta\varphi = 0$ and $\cos\Delta\varphi = 1$ into the matrix and simplifying it, we obtain the matrix Ei that represents the transformation of the rotational joint clearance error as follows:

$$E_i = \begin{bmatrix} 1 & -\Delta\phi_z^i & \Delta\phi_y^i & \Delta x_i \\ \Delta\phi_z^i & 1 & -\Delta\phi_x^i & \Delta y_i \\ -\Delta\phi_y^i & \Delta\phi_x^i & 1 & \Delta z_i \\ 0 & 0 & 0 & 1 \end{bmatrix} \tag{4}$$

The text describes the clearance error in a sliding joint. In Fig. 5, the lower end of the pin shaft is fixed on the slider of a stepper motor, allowing the pin shaft to move in the direction shown in the diagram. Fig. 6 is a top view of the dashed portion in Fig. 5. To ensure smooth sliding of the pin shaft within the slider under the control of the stepper motor, there is a certain gap between the pin shaft and the bottom plate's slot. When the stepper motor operates, it drives the pin shaft to undergo displacement. The pin shaft body collides and experiences friction with the inner side of the bottom plate's slot. As a result, the bottom plate exhibits additional rotational error around the rotational axis on its right side. The maximum value of the additional rotational error angle β caused by the clearance in the sliding joint can be calculated using the following formula.

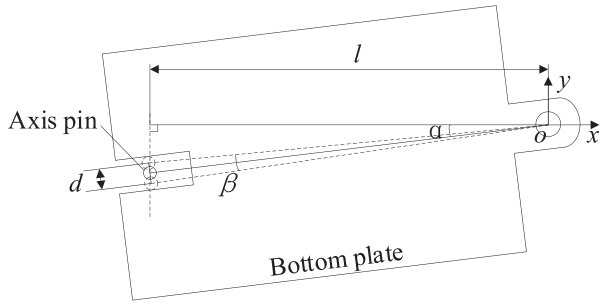

Fig. 7. Influence of base plate sliding friction pair clearance.

Assume that the right side rotational axis is fixed and the connection between the rotational axis and the bottom plate is modelled as an ideal rotating sub-model with no clearance. Then as shown in Fig. 7, the z-axis of the set coordinate system coincides with the axis of the right rotary axis, and the x-axis and *y*-axis are parallel to the two sides of the base plate. It is known that the pin axis in parallel with the *yoz* plane and distance l from the *yoz* plane along the y-axis direction to do linear motion, assuming that at this moment the pin axis distance from the two sides of the slide groove is equal, the value of *d*/2, and in the plane shown in the pin axis and the axis of the right-hand side of the axis of the axis of the rotary axis of the connecting line with the x-axis angle of α, then can be approximated to find out the maximum value of the base plate in the freedom around the axis of the right-hand side of the axis of the rotary additional rotational error angle β. That is, in the horizontal plane, the When the axis of the pin axis and the axis of the bottom plate axis of rotation is located in a straight line and the *x*-axis angle is α, the maximum value of the additional rotation error angle β of the base plate generated by the sliding friction vice clearance around the right axis of rotation is calculated as follows:

$$\beta = 2\arctan\left(\frac{d\cos\alpha}{2l}\right) \tag{5}$$

$$RPY(\Delta\phi_x^i, \Delta\phi_y^i, \Delta\phi_z^i) = \begin{bmatrix} c\Delta\phi_z^i c\Delta\phi_y^i & c\Delta\phi_z^i s\Delta\phi_y^i s\Delta\phi_x^i - s\Delta\phi_z^i c\Delta\phi_x^i & c\Delta\phi_z^i s\Delta\phi_y^i c\Delta\phi_x^i + s\Delta\phi_z^i s\Delta\phi_x^i & 0 \\ s\phi_z^i c\Delta\phi_y^i & s\Delta\phi_z^i s\Delta\phi_y^i s\Delta\phi_x^i + c\Delta\phi_z^i c\Delta\phi_x^i & s\Delta\phi_z^i s\Delta\phi_y^i c\Delta\phi_x^i - c\Delta\phi_z^i s\Delta\phi_x^i & 0 \\ -s\Delta\phi_y^i & c\Delta\phi_y^i s\Delta\phi_x^i & c\Delta\phi_y^i c\Delta\phi_x^i & 0 \\ 0 & 0 & 0 & 1 \end{bmatrix} \tag{2}$$

$$\begin{aligned} E_i &= M(\Delta x_i, \Delta y_i, \Delta z_i) RPY(\Delta\phi_x^i, \Delta\phi_y^i, \Delta\phi_z^i) \\ &= \begin{bmatrix} c\Delta\phi_z^i c\Delta\phi_y^i & c\Delta\phi_z^i s\Delta\phi_y^i s\Delta\phi_x^i - s\Delta\phi_z^i c\Delta\phi_x^i & c\Delta\phi_z^i s\Delta\phi_y^i c\Delta\phi_x^i + s\Delta\phi_z^i s\Delta\phi_x^i & \Delta x_i \\ s\Delta\phi_z^i c\Delta\phi_y^i & s\Delta\phi_z^i s\Delta\phi_y^i s\Delta\phi_x^i + c\Delta\phi_z^i c\Delta\phi_x^i & s\Delta\phi_z^i s\Delta\phi_y^i c\Delta\phi_x^i - c\Delta\phi_z^i s\Delta\phi_x^i & \Delta y_i \\ -s\Delta\phi_y^i & c\Delta\phi_y^i s\Delta\phi_x^i & c\Delta\phi_y^i c\Delta\phi_x^i & \Delta z_i \\ 0 & 0 & 0 & 1 \end{bmatrix} \end{aligned} \tag{3}$$

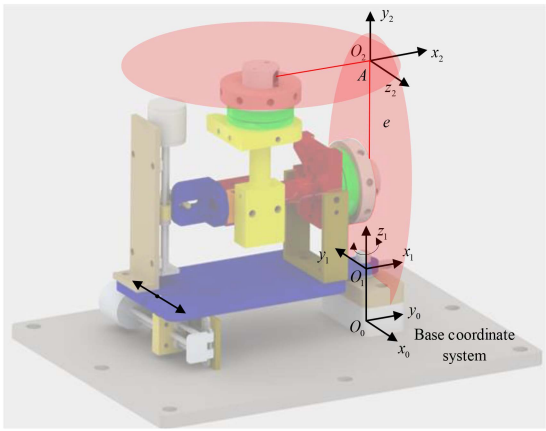

Fig. 8. Spatial position of each coordinate system.

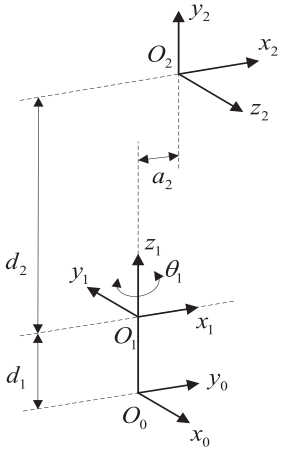

Fig. 9. Transformation process of D-H parameter method.

In order to determine the positions of each coordinate system according to the D-H parameter convention, we start by establishing the position and orientation of the base coordinate system O_0-$x_0y_0z_0$ on the bottom plate, as shown in Fig. 8.

Based on the spatial positions of the various coordinate systems mentioned above, we can obtain the D-H parameter transformation process as shown in Fig. 9.

By taking $i = 1{,}2$ successively, we can obtain the transformation matrices ${}^0T_1$ and ${}^1T_2$. Here, θ_1 represents the variable rotational angle of the revolute joint during the motion of the mechanism. The results are as follows:

$$ {}^0T_1 = \begin{bmatrix} c\theta_1 & -s\theta_1 & 0 & 0 \\ s\theta_1 & c\theta_1 & 0 & 0 \\ 0 & 0 & 1 & d_1 \\ 0 & 0 & 0 & 1 \end{bmatrix} \tag{6} $$

$$ {}^1T_2 = \begin{bmatrix} 1 & 0 & 0 & a_2 \\ 0 & 0 & -1 & 0 \\ 0 & 1 & 0 & d_2 \\ 0 & 0 & 0 & 1 \end{bmatrix} \tag{7} $$

In the above formulas, 'c' represents the simplified symbol for cosine, and 's' represents the simplified symbol for sine.

By multiplying the aforementioned transformation matrices in sequence, we can obtain the transformation matrix ${}^0T_2$ from the motion coordinate system O_2-$x_2y_2z_2$ to the base coordinate system O_0-$x_0y_0z_0$. This matrix can also represent the pose matrix of the cross laser emitted during the transverse adjustment process of the laser emitter in the base coordinate system O_0-$x_0y_0z_0$. This matrix represents the motion model of the cross laser emitted by the laser emitter during the transverse adjustment process without considering errors [11]. The computation results are as follows:

$$ {}^0T_2 = {}^0T_1\,{}^1T_2 = \begin{bmatrix} c\theta_1 & 0 & s\theta_1 & a_2c\theta_1 \\ s\theta_1 & 0 & -c\theta_1 & a_2s\theta_1 \\ 0 & 1 & 0 & d_1 + d_2 \\ 0 & 0 & 0 & 1 \end{bmatrix} \tag{8} $$

Now let's consider the influence of joint clearance on the pose of the cross laser and establish the joint error transmission model for the transverse laser emitter. In the process of transverse adjustment of the laser emitter, assuming that the vertical stepper motor is not engaged, and assuming no clearance or relative motion between the sliding joint of the vertical stepper motor driving part and the laser pen frame and bracket, we only need to consider the influence of clearance in the rotational joint at the bottom plate rotational axis and the sliding joint at the horizontal stepper motor. The transformation matrix associated with the clearance error of the rotational joint, denoted as E_i, can be applied to the coordinate transformation matrix ${}^0T_1$ under the absence of any joint clearance by right-multiplying E_1. The calculation expression for ${}^0T_1^{E\ \ Rot}$ under the influence of the rotational joint clearance at the bottom plate rotational axis is as follows: (9) shown at the bottom of the next page.

Under the influence of the clearance in the sliding joint of the stepper motor driving part, additional rotational errors occur in the controlled rotational joint of that motor, with a maximum error angle of β_1. Therefore, under the influence of the sliding joint clearance, additional rotational errors around the z_1-axis occur at the bottom plate rotational axis. This effect can be transformed into additional rotation around the bottom plate rotational axis, with an angle of γ_1. Thus, the error matrix E_1^{slip} caused by the clearance in the sliding joint at the horizontal stepper motor is as follows:

$$ E_1^{slip} = \begin{bmatrix} \cos\gamma_1 & -\sin\gamma_1 & 0 & 0 \\ \sin\gamma_1 & \cos\gamma_1 & 0 & 0 \\ 0 & 0 & 1 & 0 \\ 0 & 0 & 0 & 1 \end{bmatrix} \tag{10} $$

The value of angle γ_1 does not exceed the maximum error angle β_1. Since the rotational error angle generated by the sliding joint clearance is small, we can approximate $\sin\gamma_1$ as γ_1 and $\cos\gamma_1$ as 1. Simplifying the error matrix E_1^{slip}, we have:

$$ E_1^{slip} = \begin{bmatrix} 1 & -\gamma_1 & 0 & 0 \\ \gamma_1 & 1 & 0 & 0 \\ 0 & 0 & 1 & 0 \\ 0 & 0 & 0 & 1 \end{bmatrix} \tag{11} $$

To obtain the transformation matrix from coordinate system $\{0\}$ to coordinate system $\{1\}$ considering the combined effects

of the sliding joint clearance error and the rotational joint clearance error at the bottom plate rotational axis, we can multiply the error matrix E1 obtained for the horizontal stepper motor by the coordinate transformation matrix ${}^0T_1^{E\ Rot}$. The expression for calculating the transformation matrix ${}^0T_1^E$ is as follows:

$$ {}^0T_1^E = {}^0T_1^{E\ Rot} E_1^{slip} \tag{12}$$

To derive the joint error transfer matrix ${}^0T_2^E$ for the transverse laser emitter, considering the combined effects of the sliding joint clearance error and the rotational joint clearance error, you need to multiply the transformation matrix ${}^0T_1^E$ obtained previously with the transformation matrices of the adjacent coordinate systems. The resulting expression for ${}^0T_2^E$ is as follows:

$$ {}^0T_2^E = {}^0T_1^{E1}T_2^E = {}^0T_1 E_1 E_1^{slip1} T_2 \tag{13}$$

In the longitudinal adjustment process of the laser emitter, where the transverse stepper motor is not in operation, only the impact of clearance errors during the control of the bottom plate rotation by the transverse stepper motor on the pose of the cross laser needs to be considered. Therefore, in the motion model of the transverse adjustment process of the laser emitter, we can neglect the effects of clearance between the vertical stepper motor-driven sliding joint and the rotational joint between the laser pen bracket and the bracket. The clearances that need to be considered are only the rotational joint clearance between the bottom plate rotational axis and the bottom plate and the sliding joint clearance between the transverse stepper motor controlled pin shaft and the slideway.

Taking $i = 12{,}3$ successively, we obtain the transformation matrix ${}^0T_3$ and ${}^3T_4$, where $\theta_3{}'$ represents the variable rotation angle of the rotational joint during the mechanism motion process. The results are as follows:

$$ {}^0T_3 = \begin{bmatrix} 0 & 0 & 1 & 0 \\ c\theta_3{}' & -s\theta_3{}' & 0 & a_3 \\ s\theta_3{}' & c\theta_3{}' & 0 & l_3 \\ 0 & 0 & 0 & 1 \end{bmatrix} \tag{14}$$

$$ {}^3T_4 = \begin{bmatrix} 0 & 0 & 1 & 0 \\ 1 & 0 & 0 & a_4 \\ 0 & 1 & 0 & b_4 \\ 0 & 0 & 0 & 1 \end{bmatrix} \tag{15}$$

In the above equations, 'c' denotes the simplified symbol for cosine, and 's' denotes the simplified symbol for sine.

By multiplying the transformation matrices mentioned above in sequence, we can obtain the transformation matrix ${}^0T_4$ from the motion coordinate system O_4-$x_4y_4z_4$ to the base coordinate system O_0-$x_0y_0z_0$. This matrix represents the pose of the transverse laser plane emitted by the longitudinal laser emitter in the base coordinate system O_0-$x_0y_0z_0$. In other words, it represents the motion model of the laser emitter under different joint angles without considering errors. The calculation results are as follows:

$$ {}^0T_4 = {}^0T_3{}^3T_4 = \begin{bmatrix} 0 & 1 & 0 & b_4 \\ -s\theta_3{}' & 0 & c\theta_3{}' & -a_4 s\theta_3{}' + a_3 \\ c\theta_3{}' & 0 & s\theta_3{}' & a_4 c\theta_3{}' + l_3 \\ 0 & 0 & 0 & 1 \end{bmatrix} \tag{16}$$

Earlier, we completed the establishment of the longitudinal laser emitter motion model without considering the influence of motion joint clearances. Now, we are considering the effect of motion joint clearances on the pose of the cross laser and developing a joint error transmission model for the longitudinal laser emitter. In the longitudinal adjustment process of the laser emitter, the horizontal stepper motor is not functioning. Assuming there are no clearances or relative motion between the sliding joint of the horizontal stepper motor drive and the rotation joint at the bottom plate, we only need to consider the influence of clearances in the rotating joint between the laser pen frame and the bracket, as well as the sliding joint clearance at the vertical stepper motor.

Given the transformation matrix E_i generated by the clearance error in the rotating joint, the coordinate transformation matrix ${}^0T_3^{E\ Rot}$ under the influence of the clearance in the rotating joint at the laser pen frame's rotational axis can be obtained by right-multiplying E_3 with the coordinate transformation matrix ${}^0T_3$ without the effects of joint clearances. The calculation method for obtaining the expression of ${}^0T_3^{E\ Rot}$ is as follows:

$$ {}^0T_3^{E\ Rot} = {}^0T_3 E_3 \tag{17}$$

Under the influence of the clearance in the sliding joint of the horizontal stepper motor drive, additional rotational errors occur in the controlled rotating joint of the motor, with a maximum error angle of β_3. Consequently, the influence of the sliding joint clearance results in an additional rotational error around the z_3 axis at the rotational axis of the laser pen frame. This influence can be converted into an additional rotation around the bottom plate rotational axis, with a rotational angle of γ_3. Therefore, the error matrix E_3^{slip} generated by the clearance in the sliding joint at the horizontal stepper motor can be described as follows:

$$ E_3^{slip} = \begin{bmatrix} \cos\gamma_3 & -\sin\gamma_3 & 0 & 0 \\ \sin\gamma_3 & \cos\gamma_3 & 0 & 0 \\ 0 & 0 & 1 & 0 \\ 0 & 0 & 0 & 1 \end{bmatrix} \tag{18}$$

The angle γ_3 is limited to not exceed the maximum error angle β_3. Since the rotational error angle generated by the sliding joint clearance is very small, we can approximate $\sin\gamma_3$ as γ_3 and

$$ {}^0T_1^{E\ Rot} = {}^0T_1 E_1 = \begin{bmatrix} c\theta_1 - s\theta_1\Delta\phi_z^1 & -c\theta_1\Delta\phi_z^1 - s\theta_1 & c\theta_1\Delta\phi_y^1 + s\theta_1\Delta\phi_x^1 & \Delta x_1 c\theta_1 - \Delta y_1 s\theta_1 \\ s\theta_1 + \Delta\phi_z^1 c\theta_1 & -\Delta\phi_z^1 s\theta_1 + c\theta_1 & \Delta\phi_y^1 s\theta_1 - \Delta\phi_x^1 c\theta_1 & \Delta x_1 s\theta_1 + \Delta y_1 c\theta_1 \\ -\Delta\phi_y^1 & \Delta\phi_x^1 & 1 & d_1 + \Delta z_1 \\ 0 & 0 & 0 & 1 \end{bmatrix} \tag{9}$$

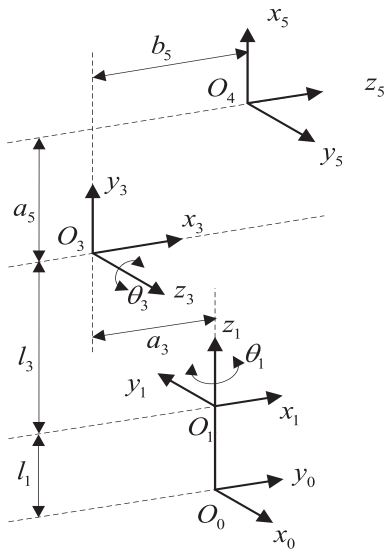

Fig. 10. Transformation process of D-H parameter method.

cosγ_3 as 1. Therefore, the error matrix E_3^{slip} can be simplified as follows:

$$E_3^{slip} = \begin{bmatrix} 1 & -\gamma_3 & 0 & 0 \\ \gamma_3 & 1 & 0 & 0 \\ 0 & 0 & 1 & 0 \\ 0 & 0 & 0 & 1 \end{bmatrix} \tag{19}$$

By right-multiplying the error matrix E_3^{slip} generated by the sliding joint clearance at the horizontal stepper motor with the coordinate transformation matrix ${}^0T_3^{E\ Rot}$ that considers the influence of the rotation joint clearance at the bottom plate, we can obtain the expression of the coordinate transformation matrix ${}^0T_3^E$ from the coordinate system {0} to the coordinate system {3} under the combined influence of the sliding joint clearance error and the rotation joint clearance error. The calculation for obtaining the expression of the coordinate transformation matrix ${}^0T_3^E$ is as follows:

$${}^0T_3^E = {}^0T_3^{E\ \ Rot}E_3^{slip} \tag{20}$$

To derive the joint error transfer matrix ${}^0T_4^E$ for the longitudinal laser emitter, considering the combined effects of the sliding joint clearance error and the rotational joint clearance error, you need to multiply the transformation matrix ${}^0T_3^E$ obtained previously with the transformation matrices of the adjacent coordinate systems. The resulting expression for ${}^0T_4^E$ is as follows:

$${}^0T_4^E = {}^0T_3^{E3}T_4^E = {}^0T_3^{E3}T_4 = {}^0T_3E_3E_3^{slip3}T_4 \tag{21}$$

III. Dual-Axis Coupling Model

Based on the spatial positions of the respective coordinate systems mentioned above, the D-H parameter method transformation process, as shown in Fig. 10 can be obtained [12].

By sequentially considering i = 1,2,3, the transformation matrices ${}^0T_1$, ${}^1T_3$, and ${}^3T_5$ can be obtained. In the transformation matrix ${}^1T_2$, an additional rotation matrix *Rot* is needed to represent the rotation at the laser pen axis, with an angle θ_2. The variables θ_1 and θ_2 in the coordinate system represent the rotational angles of the rotary joint during the mechanical motion process, and the values inside the parentheses denote the initial values. The results are as follows:

$${}^0T_1 = \begin{bmatrix} c\theta_1 & -s\theta_1 & 0 & 0 \\ s\theta_1 & c\theta_1 & 0 & 0 \\ 0 & 0 & 1 & l_1 \\ 0 & 0 & 0 & 1 \end{bmatrix} \tag{22}$$

$${}^1T_3 = \begin{bmatrix} c\theta_3 & -s\theta_3 & 0 & a_3 \\ 0 & 0 & -1 & 0 \\ s\theta_3 & c\theta_3 & 0 & l_3 \\ 0 & 0 & 0 & 1 \end{bmatrix} \tag{23}$$

$${}^3T_5 = \begin{bmatrix} 0 & 0 & 1 & b_5 \\ 1 & 0 & 0 & a_5 \\ 0 & 1 & 0 & 0 \\ 0 & 0 & 0 & 1 \end{bmatrix} \tag{24}$$

In the above equations, 'c' is a shorthand for cosine, and 's' is a shorthand for sine.

By multiplying the aforementioned transformation matrices sequentially, we can obtain the transformation matrix ${}^0T_5$ from the motion coordinate system O_5-$x_5y_5z_5$ to the base coordinate system O_0-$x_0y_0z_0$ without considering the effects of errors. This represents the motion model of the laser emitter under different joint angles without considering errors.

$$\begin{aligned} {}^0T_5 &= {}^0T_1{}^1T_3{}^3T_5 \\ &= \begin{bmatrix} -c\theta_1s\theta_2 & s\theta_1 & c\theta_1c\theta_2 & b_5c\theta_1c\theta_2 - a_5c\theta_1s\theta_2 + a_3c\theta_1 \\ -s\theta_1s\theta_2 & -c\theta_1 & s\theta_1c\theta_2 & b_5s\theta_1c\theta_2 - a_5s\theta_1s\theta_2 + a_3s\theta_1 \\ c\theta_2 & 0 & s\theta_2 & b_5s\theta_2 + a_5c\theta_2 + l_1 + l_3 \\ 0 & 0 & 0 & 1 \end{bmatrix} \end{aligned} \tag{25}$$

The influence of joint clearances on the cross laser formed by the intersection of horizontal and vertical lasers needs to consider the combined effects of the sliding joint clearance at the horizontal stepper motor drive pin, the rotation joint clearance at the bottom plate rotational axis, the sliding joint clearance at the vertical stepper motor drive pin, and the rotation joint clearance at the laser pen axis.

In the laser emitter model, it is known that the effects of two rotation joint clearance errors act on coordinate systems O_1-$x_1y_1z_1$ and O_3-$x_3y_3z_3$ respectively. When adjusting the longitudinal laser using the horizontal stepper motor and the vertical stepper motor, additional rotations around the z_1 and z_3 axes are caused by the presence of sliding joint, affecting the coordinate systems O_1-$x_1y_1z_1$ at the bottom plate and O_3-$x_3y_3z_3$ at the laser pen rack, respectively.

In Chapter II, the calculation formula for the transformation matrix ${}^{i-1}T_i^E$ from coordinate system {i-1} to coordinate system {i} under the combined influence of sliding joint clearance error and rotation joint clearance error has been derived. By multiplying the calculated transformation matrices of adjacent coordinate systems sequentially, the joint error transmission model of the transverse laser emitter ${}^0T_5^E$ can be obtained as follows:

$${}^0T_5^E = {}^0T_1^{E1}T_3^{E3}T_5 = {}^0T_1E_1E_1^{slip1}T_3E_3E_3^{slip3}T_5 \tag{26}$$

In the above equation:

$$
{}^{0}T_{1} = \begin{bmatrix} \mathrm{c}\theta_1 & -\mathrm{s}\theta_1 & 0 & 0 \\ \mathrm{s}\theta_1 & \mathrm{c}\theta_1 & 0 & 0 \\ 0 & 0 & 1 & l_1 \\ 0 & 0 & 0 & 1 \end{bmatrix},
$$

$$
E_1 = \begin{bmatrix} 1 & -\Delta\phi_z^1 & \Delta\phi_y^1 & \Delta x_1 \\ \Delta\phi_z^1 & 1 & -\Delta\phi_x^1 & \Delta y_1 \\ -\Delta\phi_y^1 & \Delta\phi_x^1 & 1 & \Delta z_1 \\ 0 & 0 & 0 & 1 \end{bmatrix}
$$

$$
E_1^{slip} = \begin{bmatrix} \cos\gamma_1 & -\sin\gamma_1 & 0 & 0 \\ \sin\gamma_1 & \cos\gamma_1 & 0 & 0 \\ 0 & 0 & 1 & 0 \\ 0 & 0 & 0 & 1 \end{bmatrix},
$$

$$
{}^{1}T_{3} = \begin{bmatrix} c\theta_3 & -s\theta_3 & 0 & a_3 \\ 0 & 0 & -1 & 0 \\ s\theta_3 & c\theta_3 & 0 & l_3 \\ 0 & 0 & 0 & 1 \end{bmatrix}
$$

$$
E_3 = \begin{bmatrix} 1 & -\Delta\phi_z^3 & \Delta\phi_y^3 & \Delta x_3 \\ \Delta\phi_z^3 & 1 & -\Delta\phi_x^3 & \Delta y_3 \\ -\Delta\phi_y^3 & \Delta\phi_x^3 & 1 & \Delta z_3 \\ 0 & 0 & 0 & 1 \end{bmatrix},
$$

$$
E_3^{slip} = \begin{bmatrix} 1 & -\gamma_3 & 0 & 0 \\ \gamma_3 & 1 & 0 & 0 \\ 0 & 0 & 1 & 0 \\ 0 & 0 & 0 & 1 \end{bmatrix}
$$

Through the analysis of the error sources in the laser emitter, it is known that the joint clearance error belongs to random error. Based on the characteristics of random error, it can be inferred that most random errors follow a certain distribution pattern. Therefore, the distribution of joint clearance errors will be analyzed below.

According to general principles, joint clearance errors follow a normal distribution. In order to ensure a confidence level of 99% or higher for the obtained joint clearances, according to the 3σ rule, the size of the clearance error follows a normal distribution with a mean of μ_i and a standard deviation of σ_i. The calculations for these variables are as follows [13]: (27) shown at the bottom of this page.

The rotation joint clearance error can be divided into radial error and axial error based on the direction of the error. The radial error value is the difference between the joint hole diameter and the joint shaft diameter, while the axial error is the tolerance value of the axial constraint section size of the rotating joint component. The bottom plate rotational axis provides support for the bottom plate, bracket, laser pen rack, and rotating motor, and it has certain positioning accuracy requirements. Therefore, H6/g5 clearance fit can be considered based on practical considerations. The basic dimension of the shaft is known to be 8 mm, with a hole tolerance grade of H6 and a shaft tolerance grade of g5. The thickness of the bottom plate is 5 mm, and the tolerance of the component can be determined based on the commonly used tolerance grade of IT7.The diameter of the shaft at the laser pen rack rotational axis is 2.5 mm, and the diameter of the hole in the bracket is 3 mm. The standard dimension of the contact section between the inner side of the bracket and the laser pen rack is 38 mm, with a tolerance grade of IT7.

The sliding joint is achieved by the cooperation between the pin shaft and the sliding groove, enabling the rotation of the bottom plate and the laser pen rack driven by two stepper motors, respectively. Considering the slide of the pin shaft in the sliding groove and cost-saving measures, an H9/c9 shaft-hole clearance fit, which provides relatively large clearance, can be employed. The basic dimension of the two pin shafts is known to be 3 mm, with a hole tolerance grade of H9 and a shaft tolerance grade of c9.

In the initial state of the device, it is known that joint one has a rotation angle θ_1^0 of $\pi/2$, and joint two has a rotation angle θ_3^0 of 0. By setting the rotation angle for joint one, θ_1, to $\pm\pi/12$, and the transformation angle for joint two, θ_3 to $\pm\pi/9$, we can obtain the range of values for joint variables: $\theta_1 = (5\pi/12, 7\pi/12)$ and $\theta_2 = (-\pi/9, \pi/9)$.

Using MATLAB programming simulation and inputting the joint variables and the values of the D-H parameters, we can obtain the transformation matrix ${}^{0}T_5$, which represents the transformation from the coordinate system {5} to the base coordinate system {0}. This matrix allows us to determine the changes in the coordinates (x, y, z) of the end effector in the base coordinate system, without considering the influence of clearance errors.

By performing calculations in MATLAB, we can obtain the distribution of the end effector's positions in the base coordinate system when clearance errors are not considered. The spatial distribution of the end effector in the base coordinate system, as well as the views along the x-axis, y-axis, and z-axis directions, can be visualized and depicted as shown in Fig. 11.

By incorporating the normal distribution of axial clearances, radial clearances, and rotational errors around each axis into the actual transformation matrix ${}^{0}T$E 5, which takes into account the effects of clearance errors between motion joint, we can obtain the positional distribution of the end point in the base coordinate system considering the error influences (represented by blue dots). By overlaying this output image with the positional distribution of the end point in the base coordinate system without considering the effects of motion joint clearance error (represented by red dots), we can generate a comparative image that shows the positional distribution of the end point in the base coordinate system with and without considering the effects of motion joint clearance errors. The spatial positional distribution and the views along the x-axis, y-axis, and z-axis are shown in Fig. 12.

The comparison of the spatial distribution of the end point with and without errors reveals that errors are more pronounced around the spatial coordinate point (0, 0, 143.7). Furthermore, to compare the motion models with and without considering

$$
\sigma_i = \frac{\mu_{\mathrm{i}}}{3} = \frac{\text{Maximum limit size of holes} - \text{Minimum limiting dimensions of the shaft}}{6} \tag{27}
$$

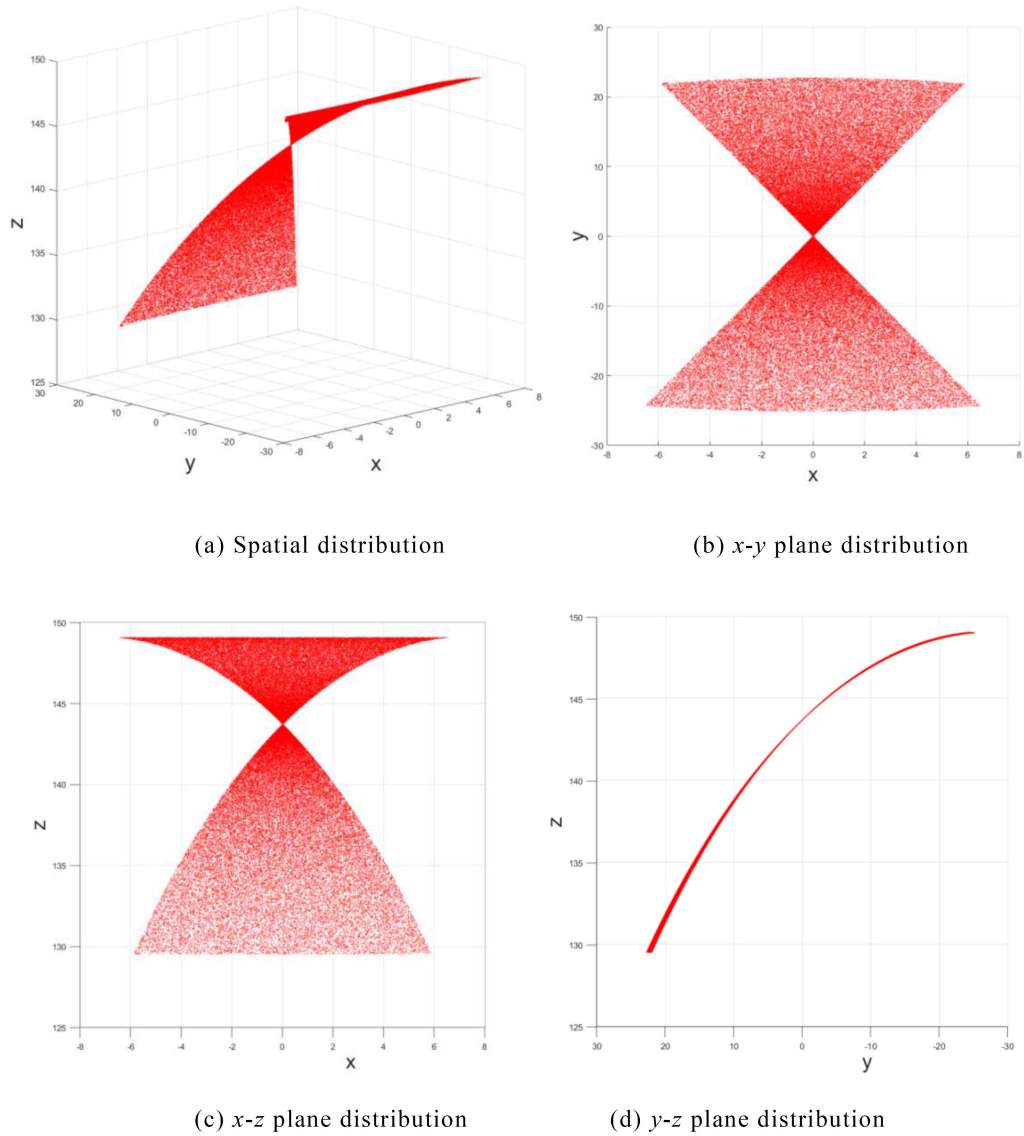

Fig. 11. Spatial distribution of end points.

motion joint clearance errors, the MATLAB program calculates the differences in the x, y, and z coordinates, considering the effects of motion joint clearance errors. These differences are then plotted as error line graphs along the x-axis, y-axis, and z-axis in Fig. 13, representing 1000 iterations. Additionally, the angular deviation values of the laser are extracted and plotted as a distribution histogram in Fig. 14.

According to Figs. 13 and 14, the error values of the cross laser in the laser emission position are mainly distributed within the range of (−2 mm, 2 mm), with the z-axis error Δz being relatively small. The angular deviation of the laser is primarily distributed in the range of 0 rad to 2.2×10^{-2} rad, accounting for 99.86% of the data, with an average deviation angle of approximately 6.673×10^{-3} rad.

Let's analyze the reason for the smaller Δz error in the z-axis direction. Taking the clearance error at the bottom plate rotation joint as an example, we will examine its impact on the cross laser error. Considering the errors generated by Joint 1, including the translational errors Δx, Δy, Δz, and the rotational errors $\Delta\varphi 1\ x$, $\Delta\varphi 1 y$, and $\Delta\varphi 1\ z$. As shown in Fig. 15, we have three coordinate systems: the base coordinate system O_0-$x_0y_0z_0$, the coordinate system O_1-$x_1y_1z_1$ representing the bottom plate rotation joint with clearance, and the coordinate system O_1-$x_1y_1z_1$ representing the cross laser. The distance along the z_1-axis is denoted as d, and the distance along the x_1-axis is denoted as a, where d $>>$ a. From the diagram, it can be observed that in the base coordinate system, the y_1-axis error caused by the rotational error $\Delta\varphi 1\ x$ is $\Delta y'$, and the z_1-axis error is $\Delta {z_1}'$. The x_1-axis error caused by $\Delta\varphi 1\ y$ is $\Delta x'$, and the z_1-axis error is $\Delta {z_2}'$. Due to the fact that d $>>$ a, the error caused by $\Delta\varphi 1\ z$ is significantly smaller than $\Delta x'$ and $\Delta y'$ (not shown in the diagram). Furthermore, since the values of rotational errors $\Delta\varphi 1\ x$, $\Delta\varphi 1\ y$, and $\Delta\varphi 1\ z$ are very small, the corresponding errors $\Delta {z_1}'$ and $\Delta {z_2}'$ are also much smaller than $\Delta x'$ and Δy'. Therefore, we can conclude that when the rotational error angles of the joint with clearance are constant, the larger the distance between the joint coordinate

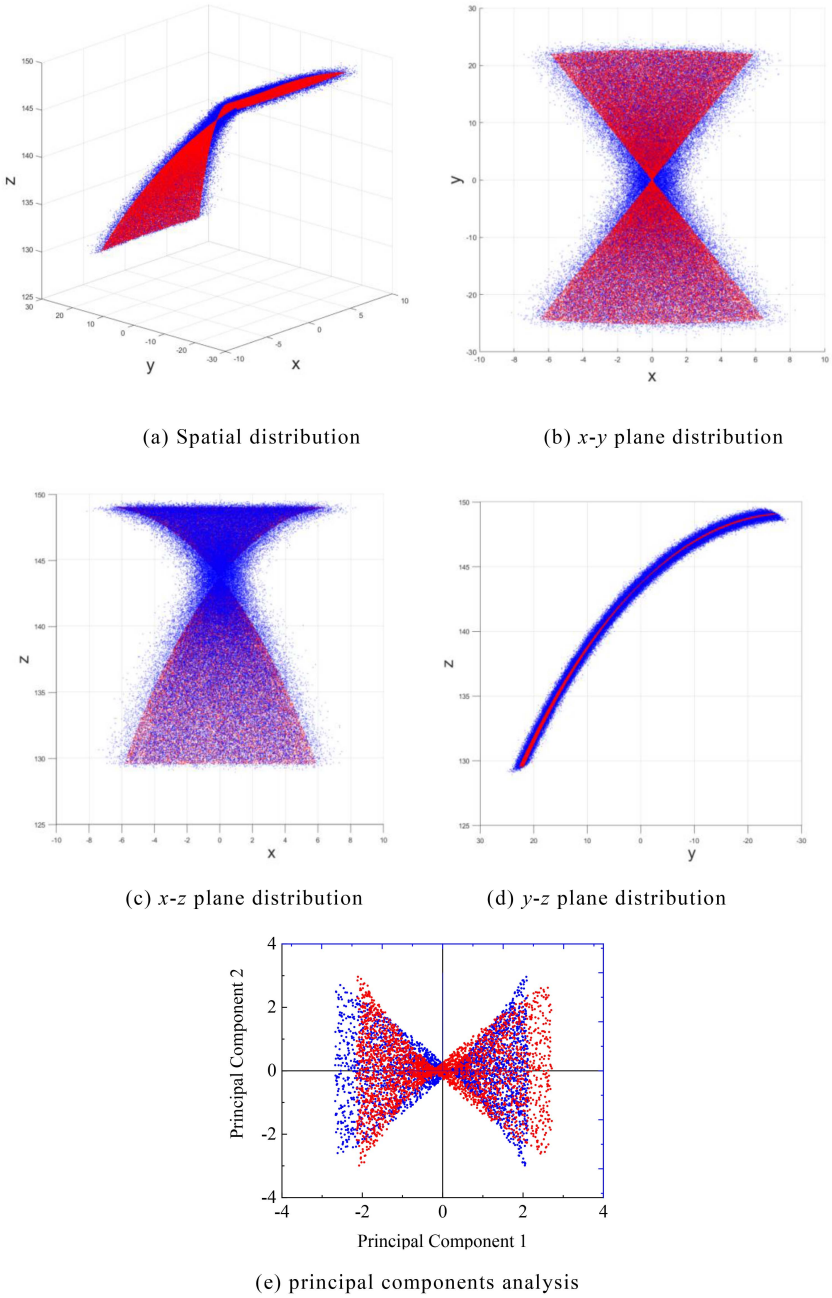

(a) Spatial distribution (b) *x*-*y* plane distribution

(c) *x*-*z* plane distribution (d) *y*-*z* plane distribution

(e) principal components analysis

Fig. 12. Spatial distribution of end point error.

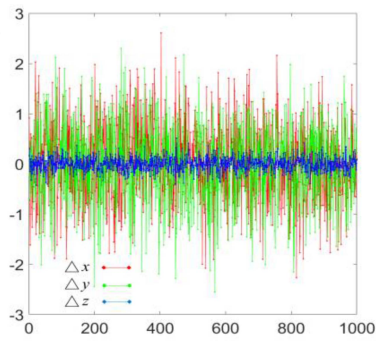

Fig. 13. Axial error distribution.

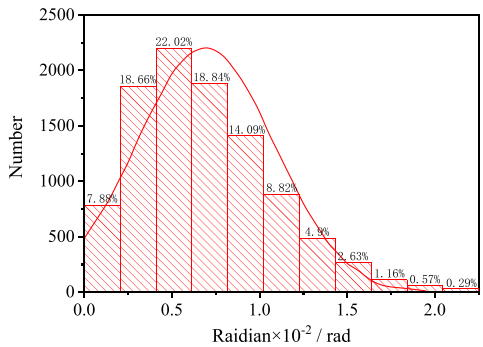

Fig. 14. Laser angle deviation distribution.

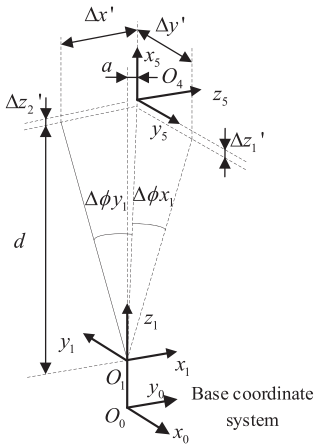

Fig. 15. Influence of clearance of base plate rotating pair on end error.

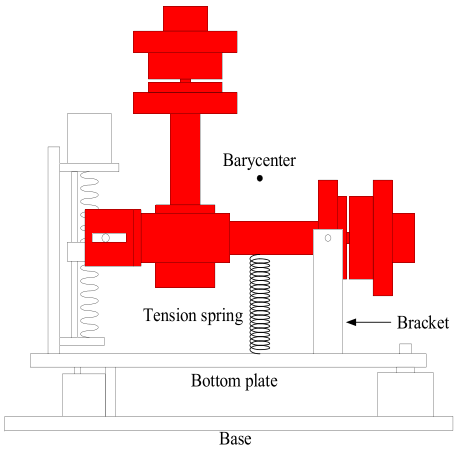

Fig. 16. Installation position of spring.

system position and the end effector coordinate system position along one axis, the greater the errors generated in the other two axes. Consequently, due to the fact that the distances along the z-axis between the bottom plate rotation joint and the laser pen holder rotation joint and their respective end effector coordinate system positions are much larger than their distances along the other two axes, the z-axis error at the end effector caused by the clearance at the three joint is much smaller compared to the errors along the x and y axes.

IV. Error Compensation Analysis

To reduce the impact of clearance in the motion joint on the positional accuracy of the cross laser, the optimization of a spring compensation method has been chosen as the research approach [14]. It is necessary to have some clearance between the components of the motion joint to ensure their mobility in certain degrees of freedom. However, when the clearance is significant, it can lead to collisions between the components during the operation of the mechanism, resulting in vibrations. By adding preloaded springs between the motion components, the separation between them can be restricted, reducing the

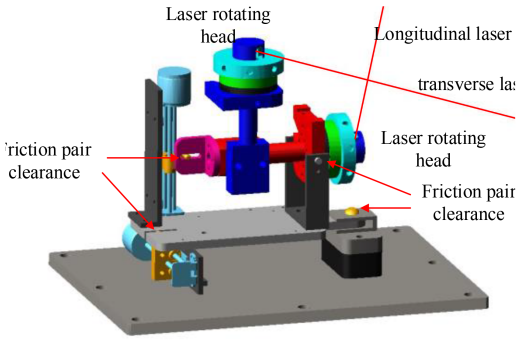

(a) Without tension spring

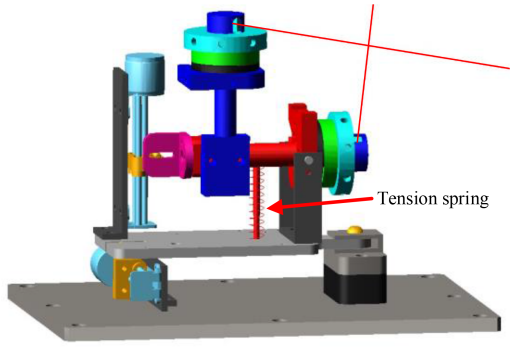

(b) With tension spring

Fig. 17. ADAMS simulation model.

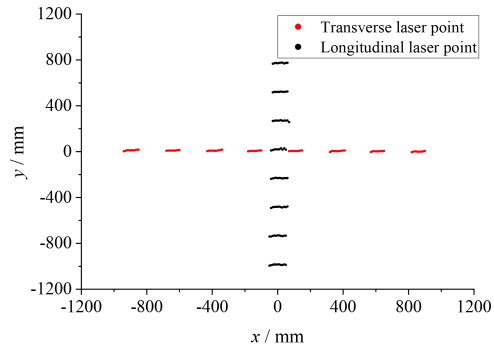

(a)Without tension spring

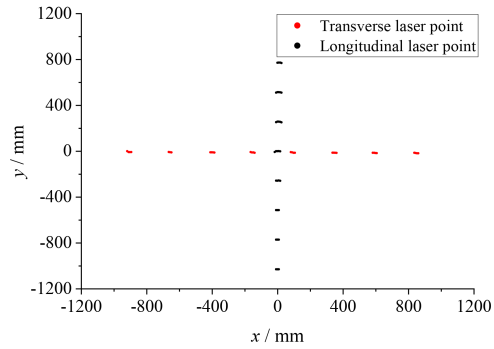

(b) With tension spring

Fig. 18. Transverse and longitudinal laser point distribution.

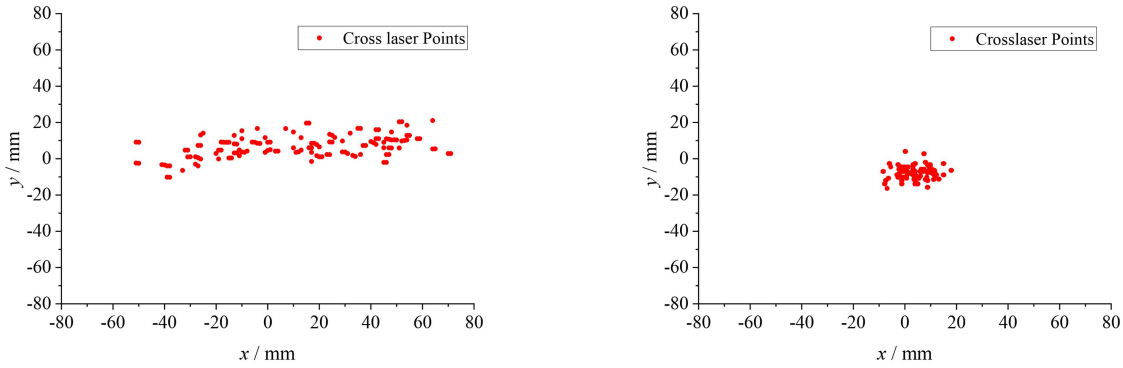

(a) Without tension spring (b) With tension spring

Fig. 19. Cross laser intersection distribution.

vibration of the components and improving the accuracy of the cross laser [15].

Among the clearances in the various motion joint of the laser emitter, the largest clearance exists at the axis of rotation of the laser pen holder, with a size of 0.5 mm. The clearances in other motion joint are smaller in value. To primarily limit the collision between components at the rotation joint of the laser pen holder, a tension spring is installed at the middle position of the transverse laser pen holder, as shown in Fig. 16. The red components in the figure include the laser pen holder, motor, and laser rotating head, which are fixed together. They are supported by the pin on the left adjustable motor slider and the rotating axis of the laser pen holder on the right. The spring mainly restricts the clearance at the rotation joint of the laser pen holder and also reduces the collision between the pin on the vertical stepper motor and the groove to some extent [15].

Import the 3D model of the laser emitter into Adams software to add constraints, and fix a line segment at the two prisms to simulate the horizontal and vertical laser emitted. It is assumed that the various moving parts in the device are well lubricated, and the influence of friction is not considered for the time being. Constraints are implemented by creating contact forces between parts that have gaps in the kinematic pair and are subject to collision. The total duration of the simulation process is 5 seconds, and the rotation speed of the two rotating motors is 20 r/s. During this period, the horizontal and vertical motors each rotate 100 times.

The two comparative simulation models are shown in Fig. 17, (a) is the initial laser emitter and (b) is the laser emitter after adding a tension spring.

Using the same method, data is filtered, and the coordinates of the laser points left on the receiver board of the cross laser 200 m away from the laser emitter are calculated for each step in the simulation. Due to the clearance between the components of the motion joint in the model and the alignment of the axes during assembly, the rotational axis is initially in a suspended state, as shown in Fig. 18. The red dot in the figure represents the transverse laser, while the black dot represents the longitudinal laser. From the figure, it can be observed that there is a larger displacement error in the x-axis direction for both the horizontal and vertical lasers, while the displacement error in the y-axis direction is smaller. Moreover, after adding the tension spring, the horizontal and vertical laser distribution range of the laser emitter along the X and Y axes is smaller, and the laser spot is more compact.

Next, these data points are filtered according to the number of revolutions. When the two rotating motors rotate the same number of revolutions, the data points where the horizontal and vertical lasers hit the laser receiver board are connected respectively. This forms the horizontal and vertical laser lines left on the laser receiver board. By recording the coordinates of the intersection point of these two laser lines, we can determine the position of the cross laser formed on the laser receiver board 200 m away when the two rotating motors complete one full revolution. As shown in Fig. 19, The cross laser without tension spring is mainly distributed in -50 to 71 mm in the x-axis direction, and -10 to 20 mm in the y-axis direction; the cross laser with tension spring is mainly distributed in the x-axis direction At -7 to 17.5 mm, it is mainly distributed at -17 to 4 mm in the y-axis direction. Comparing the two figures, it can be seen that the addition of the tension spring makes the laser distribution range of the laser transmitter along the X and Y axes smaller and the laser spots closer, which significantly improves the working stability of the laser transmitter.

Since the clearance error of the bearing in the rotating motor is not considered, the angular deviation of the cross laser during motion can be obtained by measuring the deflection angle of the laser pen holder. The obtained error angle values of the laser are plotted as a distribution histogram using Origin, as shown in Fig. 20. Based on the histogram, it can be observed that the angular deviation is mainly distributed within the range of 6 to 9×10^{-3} rad, and the average angle deviation is 7.54×10^{-3} rad; the angular deviation with tension spring is mainly distributed In the range of 0 to 13×10^{-4} rad, the average angular deviation is 5.4×10^{-4} rad, and both figures approximately obey the normal distribution law. Comparing the two figures (a) and (b), it can be seen that the addition of the tension spring significantly reduces the angular deviation range and mean deviation of the laser transmitter, and significantly improves the working stability of the laser transmitter.

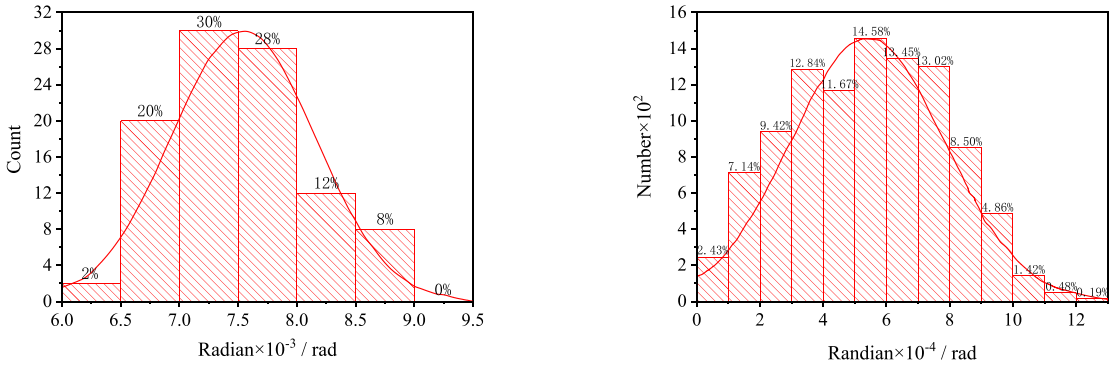

(a) Without tension spring (b) With tension spring

Fig. 20. Laser deflection angle distribution.

V. Conclusion

Based on the D-H parameter method, this paper establishes a mathematical model for the major influencing factors of laser accuracy during the adjustment process of the laser emitter in both transverse and longitudinal directions. The D-H parameter coordinate systems and the transformation matrices between adjacent coordinate systems for the transverse and longitudinal adjustment processes are determined. The mathematical model of the joint clearances is assigned values according to a normal distribution based on the size of the joint clearances and the type of joint motion. The error transmission model of the laser emitter device joint is simulated and solved. The distribution of the laser emission points in space under ideal conditions and the distribution of the laser emission points affected by joint clearances are obtained. Based on this analysis, the magnitude of errors in the laser emission points in each axis and the distribution of laser error deviation angles are determined. The method of compensating for joint errors using spring traction is proposed. By adding springs, the vibration of the joint clearances at critical points is constrained. The analysis results show that compared to current laser level instruments, the laser emitter designed in this paper has higher accuracy at the same effective distance.

References

[1] L. Rui, Z. Xin, G. Juan, and W. Miao, "Study on principle and technology of position and attitude parameters measurement system for roadheader," Environmental Science Corp., Xian, China, Rep. 20114314454258, Jul. 2011.

[2] E. M. C. Hillman and V. Voleti, "Three-dimensional imaging using swept, confocally aligned planar excitation with a powell lens and/or deliberate misalignment," U.S. Patent 2021223532A1, Jul. 22, 2021.

[3] H. Chen, W. Yang, Y. Ma, and L. Tian, "Multi-sensor fusion method for roadheader pose detection," *Mechatronics*, vol. 80, 2021, Art. no. 102669.

[4] W. Yang, "Research on laser navigation method and key technology of anchor digging machine," Ph.D. dissertation, Dept. Elect. Chi., LNT Univ., Liaoning, China, 2023.

[5] I. M. Ross and R. G. Melton, "Symmetric kinematic transformation pair using euler parameters," *J. Guid., Control, Dyn.*, vol. 10, no. 5, pp. 506–507, Sep./Oct. 1987.

[6] *Electronic Level Standard*, GB/T Standard 20920-2007, Standards Press China, Beijing, China, 2007.

[7] X. Yan, J. Shi, and M. Ling, "Design and implementation of a self balancing laser level," *Electron World*, vol. 20, pp. 148–149, 2021.

[8] L. Tian, "Research and development of automatic adjustment equipment for laser levels module," Ph.D. dissertation, Dept. Elect. Chi., YZ Univ., Jiangsu, China, 2021.

[9] A. E. Ali and A. M. Al-garni, "Evaluating the accuracy of laser levels for engineering surveying," *J. King Saud Univ.-Eng. Sci.*, vol. 8, no. 1, pp. 121–130, 1996.

[10] P. A. Jimenez and B. Shirinzadeh, "Laser interferometry measurements based calibration and error propagation identification for pose estimation in mobile robots," *Robotica*, vol. 32, pp. 165–174, Aug. 2014.

[11] X. Chen, Q. Zhang, and Y. Sun, "Non-kinematic calibration of industrial robots using a rigid–flexible coupling error model and a full pose measurement method," *Robot. Comput.-Integr. Manuf.*, vol. 57, pp. 46–58, Jun. 2019.

[12] D. Andrich and P. Pedler, "A law of ordinal random error: The rasch measurement model and random error distributions of ordinal assessments," *Measurement*, vol. 131, pp. 771–781, 2019.

[13] R. Ramesh, M. A. Mannan, and A. N. Poo, "Error compensation in machine tools — A review: Part I: Geometric, cutting-force induced and fixture-dependent errors," *Int. J. Mach. Tool Manuf.*, vol. 40, no. 9, pp. 1235–1256, Jul. 2000.

[14] M. Ahmedalbashir, L. Romdhane, and J. Lee, "Dynamics of a four-bar mechanism with clearance and springs - Modeling and experimental analysis," *J. Mech. Sci. Technol.*, vol. 31, pp. 1023–1033, Mar. 2017.

[15] L. Zhe and B. Shi, "Improving the dynamic characteristics of mechanisms with clearances using optimized springs," *J. Beijing Univ. Technol.*, vol. 4, pp. 1–6, 1990.